

INFLUENCE OF AVERAGING MASSES ON CORRELATION BETWEEN MASS-AVERAGED SAR AND TEMPERATURE RISE

A. Razmadze, L. Shoshiashvili, D. Kakulia, R. Zaridze

Tbilisi State University, Tbilisi, 0128, Georgia,

lae@laetsu.org

Abstract

The relationship between locally averaged specific absorption rate (SAR) and the corresponding steady-state temperature rise in the “Visible Human” body model exposed to plane wave at 30MHz, 75MHz, 150MHz, 450MHz, and 800MHz is investigated based on correlation analysis of their respective distributions. The spatially averaged SAR is computed using the IEEE standard SAR averaging procedure with different averaging tissue masses.

1. INTRODUCTION

Due to the rapid widespread penetration of wireless communications technology in everyday life, there has been an increasing public concern about the health implication of electromagnetic (EM) energy exposure. However, EM exposure safety has been the subject of significant research on dosimetry and possible bioeffects since the aftermath of World War II, following the introduction of powerful EM energy emitters, e.g., the radar in battlefields. Likewise safety standards have been developed by international organizations like US National Council on Radiation Protection (NCRP) [1], UK national radiation Protection Board (NRPB) [2-3], International Commission on non-Ionizing Radiation Protection (ICNIRP) [4], and the Institute of Electrical and Electronics Engineers (IEEE),

which promulgated the first exposure safety guideline in 1966 [5] and has issued numerous revisions over four decades [6-11], several of which have also been adopted by the American National Standards Institute (ANSI). Those standards and guidelines have gone through a maturation process that has recently culminated in the substantial harmonization between the most important international RF safety standards namely IEEE and ICNIRP. In fact both ICNIRP and IEEE/International Commission on Electromagnetic Safety (ICES) RF safety standards bodies, recognize the well established adverse health effects from possible excessive heating of exposed tissue. As it is shown in [12], adverse physiological effects and damage to human tissues by EM energy exposure may be induced by excessive temperature increase.

Following the consolidation of the knowledge gathered from the first few decades of RF dosimetry research [13], both whole-body and localized SAR limits were defined to protect against excessive core and spatially localized temperature increases. For what concerns the localized limits, a standard exposure metric – the spatially averaged SAR – has been defined for the averaging volumes of 1 [1, 7] and 10 grams [4, 11] of tissue, starting from different dosimetric considerations. Recently, the revised IEEE safety standard [11] has harmonized with ICNIRP on the 10-g SAR limits. However, to date, there is a paucity of systematic studies that address the relationship of spatially averaged SAR with localized temperature rise. A small number of studies have dealt with the impact of different SAR averaging volumes and schemes on the relationship with temperature rise. In [14-15], the correlation between peak spatially-averaged SAR computed using various averaging schemes and the spatial peak temperature rise is studied in relation to the human head exposure in the near-field of mobile phone-like antennas. In those papers the correlation between peak 1g and 10g SAR, using four SAR averaging schemes based on both *IEEE standard C95.3-2002* guideline [16] and ICNIRP guideline [4], and peak temperature was quantified. Those investigations have shown that peak 10g SAR computed based on IEEE

standard [16] better correlates with the related peak temperature rise. It should be noted that this conclusion was based on the correlation analysis between the peak SAR and peak temperature rise values computed in a significant number of exposure conditions, but only 1g and 10g SAR averaging masses were considered.

In contrast to the aforementioned studies, we will analyze the correlation between SAR and temperature rise for plane-wave, whole-body exposure conditions, by taking into account whole SAR and temperature distributions, whose correlation is investigated for various SAR averaging masses: 0.1, 0.5, 1, 5, 10, 20, 50, 100, and 200 grams. Since it is based on correlations among very large data sets, across several frequencies and exposure conditions, this approach allows selecting the SAR metric that correlates better, in a global sense, with the temperature distributions. The study is conducted for the plane-wave exposure at 30, 75, 150, 450 and 800 MHz, with the waves traveling along horizontal directions. For each frequency 4 cases are considered, for both vertical (E) and horizontal (H) polarizations and for 2 types of exposure: front and side (right). The coupled EM – Thermo simulations were performed using the FDTD based electromagnetic and thermal solver *FDTDLab* [17-18].

2. DOSIMETRIC MODEL AND ANALYSIS METHOD

A. Whole-Body Human Model

The numerical model used for RF exposure simulations in this study is based on Visible Human Project data sets [19] which was further segmented by researchers at the Air Force Research

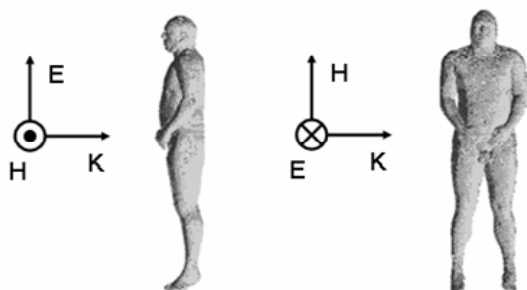


Figure. 1 Front and side (right) exposure of the human body model to plane wave

Laboratory, Brooks AFB, TX [20] to produce the voxelized model and to indicate the tissue type in each voxel. From the originally available several different resolution models

the one with 3 mm resolution (voxel dimensions: 3 x 3 x 3 mm³) has been selected to reasonably represent the body anatomy, satisfy the requirements imposed by numerical method (FDTD) [21] considering the highest frequency of RF exposure of 1.0 GHz, and to provide practical simulation time of 20 individual exposure conditions: five frequencies, front and side plane wave exposure (see Fig. 1) with both vertical (E) and horizontal (H) polarizations.

The model features 39 different tissues with electric properties taken from [22], while the thermal properties including metabolic heat production rates and blood perfusion parameters for each tissue were compiled from different sources [23-26].

B. EM Calculations Method

At present the most suitable method for the computational analysis of complex, realistic and highly inhomogeneous objects like the human body is the Finite-Difference Time-Domain (FDTD) method. The frequency-dependency of the electrical tissue parameters is determined by the four-Cole-Cole dispersion model [27]. To simulate the open space around the exposed body, the ten-layer Uniaxial Perfectly Matched Layer (UPML) method [21] has been used at the computational domain boundaries with at least 90 mm (equivalent to 30 voxels) from the body-air interface. This separation was sufficient for accurate simulations as test runs with larger UPML boundary separation from the human body model do not show significant impact on computed SAR values. Plane wave excitation and scattering has been modeled by the Total-Field Scattered-Field (TFSF) technique [21], using time-harmonic excitations at the aforementioned frequencies.

C. SAR Calculation, Averaging Scheme

For time-harmonic fields, the point-SAR is defined as:

$$SAR_{ijk} = \frac{\sigma}{2\rho} |\hat{E}|_{ijk}^2 = \frac{\sigma}{2\rho} \left(|\hat{E}_x|_{ijk}^2 + |\hat{E}_y|_{ijk}^2 + |\hat{E}_z|_{ijk}^2 \right) \quad (1)$$

where, \hat{E}_x , \hat{E}_y and \hat{E}_z are the electric field components, while σ and ρ are the tissue electrical conductivity and mass density, respectively. The 12-component averaging algorithm [28] was adopted to determine SAR values for each voxel (i, j, k) in the body model mesh. The IEEE recommended volume averaging algorithm [16] was employed to perform SAR mass-averaging. It should be observed that the air-inclusion factor is not explicitly defined in [16], though 10% is taken in this investigation, as it has been conventionally used by many researchers.

D. Thermal Calculations

The *Bio-heat* equation [29] is employed to compute the temperature rise in the body due to EM exposure, which takes into account the heat exchange mechanisms such as heat conduction, blood flow, EM energy dissipation, and metabolism

$$C_p \frac{dT}{dt} = \nabla \cdot (k \nabla T) + \rho (SAR) - B(T - T_b) + A_0 \quad (2)$$

Here, T is the point temperature, T_b is the blood temperature (assumed 36.7°C and independent of the SAR, which is an acceptable approximation as long as the basal body temperature is not changed in response to EM-induced heat), k is the thermal conductivity of the tissue, C_p the specific heat capacity, B the blood flow coefficient, and A_0 the basal metabolic heat production rate. First two member of equation 2 represent simple differential heat equation. The next member is the influence of absorbed EM energy. Another one is blood flow member, which represents the way blood with its constant

temperature acts on temperature in definite point. And the last one equation member is metabolic rate, it's constant in this model. Thermal properties are compiled from [23-26]. The convection boundary condition for (2) is used at the body-air interface:

$$H \cdot (T_s - T_c) = -K \frac{\partial T}{\partial n} \quad (3)$$

where H , T_s , and T_c denote, respectively, the convection coefficient, the body surface temperature, and the air temperature [30-31]. The convection coefficient was set to $8.4 \text{ W m}^{-2} \text{ } ^\circ\text{C}^{-1}$ [32], while the air temperature was set to 22°C .

To determine the baseline steady-state temperature distribution in the body in the absence of RF-induced heat generation, the initial steady-state temperature distribution is calculated using (2) after eliminating the electromagnetic energy absorption term. Setting the initial temperature of all tissues to 36.7°C , it would take about two hours of simulated heat diffusion and convection processes to converge to a steady-state within about $10^{-5} \text{ } ^\circ\text{C}$. The RF-induced temperature rise was then computed by taking the baseline as the initial distribution for a subsequent simulation featuring the electromagnetic energy absorption term in Eq. (2) and letting the model reach a new steady-state, also requiring about two hours of simulated heat exchange processes. It should be remarked that we normalized all SAR distributions employed in the thermal simulations to yield 2 W/kg peak 10-g average SAR, which represents the ICNIRP and the new IEEE localized exposure basic restriction for the general public. This normalization would produce peak temperature rise in the range of $0.5\text{-}0.8^\circ\text{C}$.

E. Estimate of the Correlation between SAR and Temperature Rise

One of the distinctive aspects of the approach used in this study is that a global correlation coefficient is estimated using the temperature rise and mass-averaged SAR distributions across the whole body model, not just their peak values irrespective of the geometrical proximity, for each exposure condition. This approach leads to a global

assessment of how well correlated averaged-SAR and temperature rise distributions are. The global correlation coefficient is here defined also for the case where several exposure conditions are considered together for its determination. Indicating with the index n the generic exposure condition and with m the specific averaging mass considered, the following formula is employed to derive the corresponding global correlation coefficient:

$$R^{(m)} = \frac{\sum_n \sum_{ijk} \left(SAR_{ijk,n}^{(m)} - \overline{SAR}^{(m)} \right) \left(\Delta T_{ijk,n} - \overline{\Delta T} \right)}{\sqrt{\sum_n \sum_{ijk} \left(SAR_{ijk,n}^{(m)} - \overline{SAR}^{(m)} \right)^2 \cdot \sum_n \sum_{ijk} \left(\Delta T_{ijk,n} - \overline{\Delta T} \right)^2}} \quad (4)$$

where $SAR_{ijk,n}^{(m)}$ and $\Delta T_{ijk,n}$ are the locally-averaged SAR, derived from the normalized SAR distributions for a cubic volume of mass m , and the temperature rise, respectively, at voxel (i, j, k) of the Visible Human model in the n -th exposure condition, while $\overline{SAR}^{(m)}$ and $\overline{\Delta T}$ are the ensemble SAR and temperature rise average values in the cumulative data set relative to the four plane-wave exposure conditions. To reduce the possible impact of limited simulation accuracy at points exhibiting minuscule temperature increases, voxels exhibiting $\Delta T < 0.01$ °C, well below the aforementioned peak temperature rises, have been omitted from the actual correlation estimates. Using the voxel selection criteria just described, over 2 million data points would be typically available from each modeled exposure case for the correlation analysis based on (4). The coefficient R gives possibility to evaluate how good are correlating two distributions, if coefficient R is equal to 1, they correspond ideally, if it goes to 0, they don't correlate.

3. RESULTS

Numerical simulations were carried out on an AMD Athlon™ computer equipped with a 64 X2 Dual Core 4400+ 2.21GHz processor and 3 GB memory available for electro-thermal simulations in *FDTDLab*. On Fig. 2 as an example several SAR distributions, obtained for front E-polarized plane wave exposure at 75MHz for 1, 5, 10, 50 and 100 gram

averaging masses and appropriate temperature rise are presented. For SAR averaging algorithm [16] the mass of averaging is the parameter which determines degree of smoothness. As two extreme cases point SAR and whole-body averaged SAR distributions could be considered. First is most discreet, SAR values are just obtained according equation (1) independent from each other. And in second case all the distribution is constant. All the distributions obtained for definite masses of averaging less than body mass are some kind of transitional in terms of smoothness between these two cases. For temperature it's obvious that temperature and temperature rise distributions are smooth, while values in one point can't be independent from neighbor values, system should come to steady state. That's why the idea of searching for best suited averaging mass is the idea of searching for SAR distribution which is "same way smooth" as temperature rise.

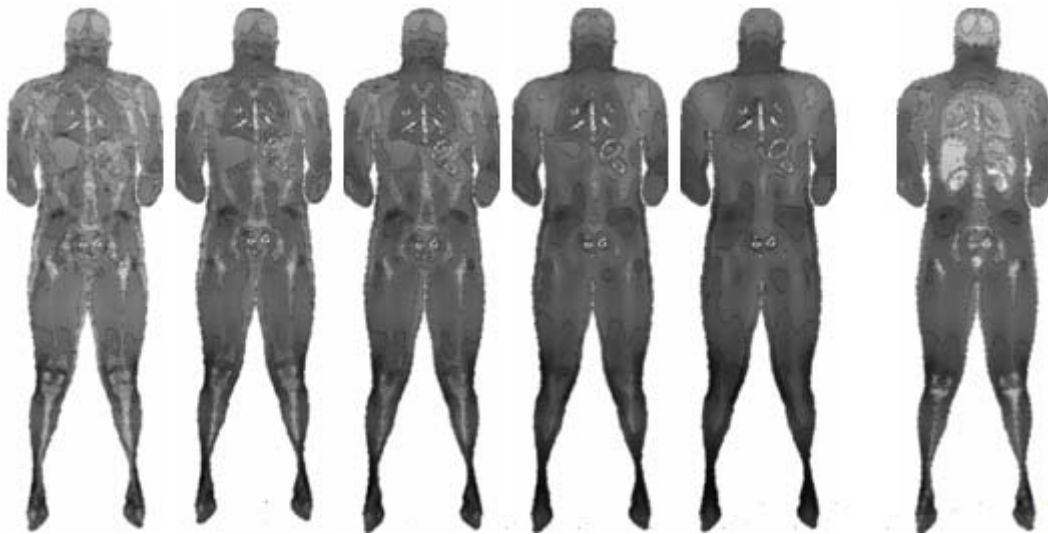


Figure 2 Example of SAR & ΔT distributions, front E-polarized plane wave exposure at 75MHz. Distributions correspond to (from left to right) 1, 5, 10, 50 and 100 grams of averaging masses. At the very right is appropriate temperature rise distribution.

As it could be noticed from Fig. 2, best correspondence between temperature rise and SAR distributions is for 5 and 10grams averaging masses, while these distributions in the best way describe by smoothness temperature rise distribution.

The correlation between the temperature rise and the corresponding spatially-averaged SAR distributions has been computed using (4). We also analyzed the dependence of the

correlation factor on various parameters, namely the frequency (including 75 MHz which is within the body resonance frequency range) and different SAR averaging masses. The results presented in Fig. 3 report the computed correlation coefficients for various frequencies and averaging masses for four plane-wave exposure conditions described earlier independently. This gives possibility to investigate independently in details behavior of correlation coefficient, it's dependence on SAR averaging mass in each exposure way.

As follows from Fig. 3, best correlation coefficient is observed for 5g averaging mass. Another observed trend is that SAR distributions appropriate to 10g averaging mass correlate always better than appropriate results for 1g averaging mass.

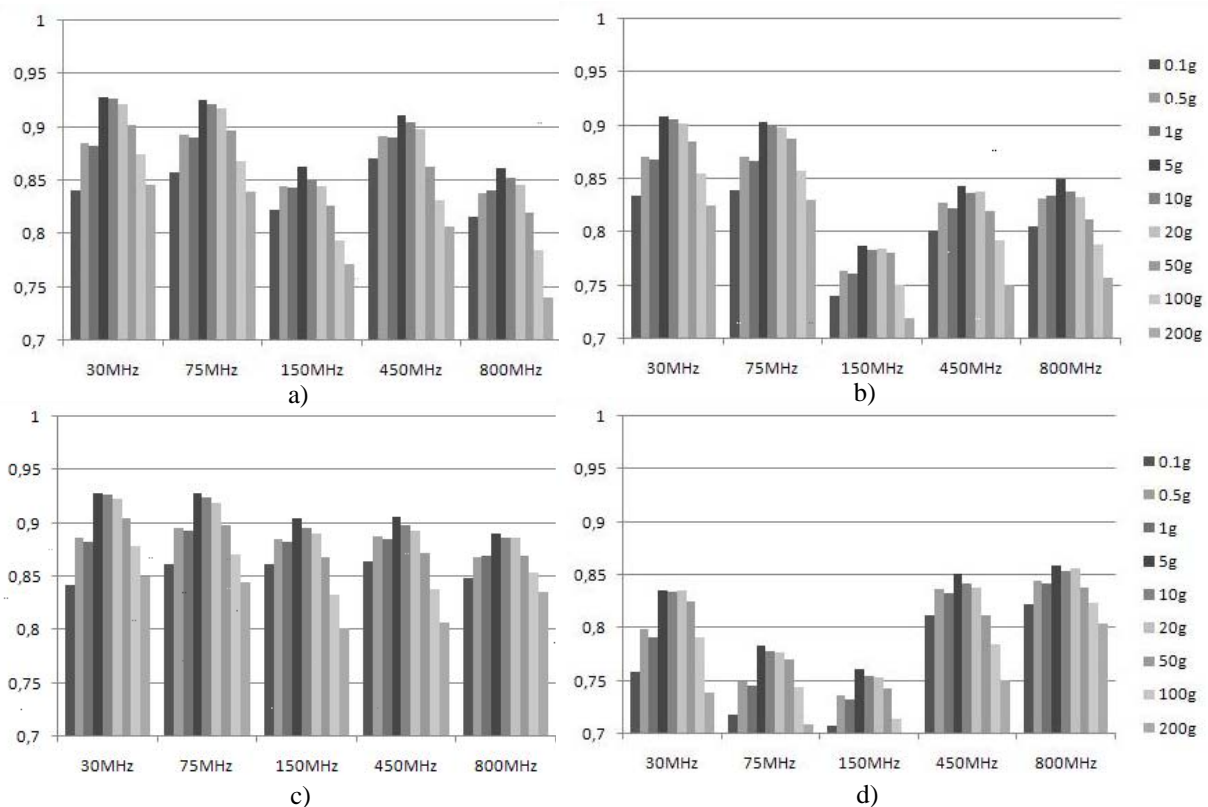


Figure 3 Correlation coefficients, based on the cumulative data set comprising the four exposure conditions independently: a) frontal plane wave exposure, E polarization, b) frontal plane wave exposure, H polarization, c) side (right) plane wave exposure, E polarization, d) side (right) plane wave exposure, H polarization

Equation (4) was employed to estimate the global correlation between the temperature rise and the corresponding mass-averaged SAR distributions, after grouping together the SAR and temperature data sets relative to the all conditions at each frequency. This grouping was deemed important to provide a robust metric incorporating the four different

body exposure conditions. In so doing, each global correlation coefficient was computed over a data set comprising more than 8 million instances. On Fig. 4 these distributions were cumulated in a single data set for each frequency and averaging masses.

Noticeably, from Fig 4., as from Fig. 3 earlier, the best correlation is obtained for 5 gram averaging mass. This result suggests that on average 5-g locally averaged SAR is the best SAR related metric to represent temperature response of the human body exposure to RF energy. Also in all cases, not depended on exposure conditions of frequency, the 10-g SAR is better correlated with the global temperature distribution than the 1-g SAR, which appears to strengthen the rationale behind the choice of the former as the basic restriction IEEE C95.1-2005 standard [16] and ICNIRP guidelines [4]. Here should be mentioned that difference between correlation coefficients for 1, 5 and 10-g averaged SAR distributions and appropriate temperature rise distributions are not more than several percents. For example, the biggest difference between 5-g and 1-g averaging masses is not more than 5% according to Figs. 3-4.

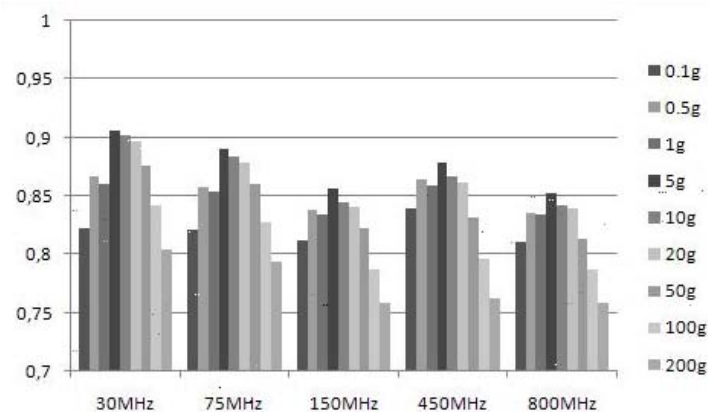


Figure 4 Global correlation coefficients, based on the cumulative data set comprising the four exposure conditions.

4. SUMMARY

This paper presents the results of the correlation analysis carried out for various locally averaged SAR and steady state temperature raise values evaluated in the human body exposed to EM field. The SAR and temperature rise data have been obtained from the numerical simulations of the realistic human body model exposure at 30MHz, 75MHz, 150MHz, 450MHz, and 800MHz in several different exposure conditions. Based on the simulated results the global correlation coefficient between and the distributions of the steady state temperature rise and the locally averaged SAR computed for different averaging tissue masses have been obtained. This approach allowed selecting the SAR averaging mass that provides the best representations of the related steady state temperature rise. The results show that in all considered exposure conditions on average the 5g SAR is the best metric in this regard, and 10g SAR is always better than 1g, which allows to make choice in favor of IEEE C95.1-2005 standard [16] in comparison with ICNIRP guidelines [4].

REFERENCES

- [1] National Council on Radiation Protection and Measurements (NCRP). Biological Effects and Exposure Criteria for Radiofrequency Electromagnetic Fields. Bethesda, MD, US (1986).
- [2] National Radiological Protection Board (NRPB). Review of the scientific evidence for limiting exposure to electromagnetic fields (0–300 GHz). Doc. NRPB, vol. 15, no. 3, Chilton, Didcot, Oxfordshire, UK (2004).
- [3] National Radiological Protection Board (NRPB). Advice on limiting exposure to electromagnetic fields (0–300 GHz). Doc. NRPB, vol. 15, no. 2, Chilton, Didcot, Oxfordshire, UK (2004).
- [4] International Commission on Non-Ionizing Radiation Protection (ICNIRP). Guidelines for limiting exposure to time-varying electric, magnetic and electromagnetic fields (up to 300GHz). Health Phys., vol. 74, pp. 494-522, 1998.
- [5] USAS C95.1-1966, Safety Level of Electromagnetic Radiation With Respect to Personnel, United States of America Standards Institute, New York, NY (1966).

- [6] ANSI C95.1-1974, Safety Level of Electromagnetic Radiation With Respect to Personnel, American National Standards Institute, New York, NY (1974).
- [7] ANSI C95.1-1982, American National Standard Safety Levels with respect to Human Exposure to Radio Frequency Electromagnetic Fields, 300 kHz to 100 GHz, American National Standards Institute, New York, NY (1982).
- [8] IEEE C95.1-1991, IEEE Standard for Safety Levels with Respect to Human Exposure to Radio Frequency Electromagnetic Fields, 3 kHz to 300 GHz, IEEE New York, NY (1991).
- [9] IEEE C95.1-1991: 1999 edition, IEEE Standard for Safety Levels with Respect to Human Exposure to Radio Frequency Electromagnetic Fields, 3 kHz to 300 GHz, IEEE New York, NY (1999).
- [10] IEEE C95.1b-2004, IEEE Standard for Safety Levels with Respect to Human Exposure to Radio Frequency Electromagnetic Fields, 3 kHz to 300 GHz - Amendment 2: Specific Absorption Rate (SAR) Limits for the Pinna, IEEE New York, NY (2004).
- [11] IEEE C95.1-2005, IEEE Standard for Safety Levels with Respect to Human Exposure to Radio Frequency Electromagnetic Fields, 3 kHz to 300 GHz, IEEE New York, NY (2005).
- [12] K. R. Foster and R. Glaser, "Thermal Mechanisms of Interaction of Radiofrequency Energy with Biological Systems with Relevance to Exposure Guidelines", *Health Physics*, 92(6):609-620, June 2007
- [13] C. H. Durney, H. Massoudi, M. F. Iskander, "Radiofrequency Radiation Dosimetry Handbook", 4th Edition, USAF Contract # F4162296P405 (Final Report), Oct. 1986 (<http://niremf.ifac.cnr.it/docs/HANDBOOK/home.htm>). [Fourth Edition]," USAF School of Aerospace Medicine, Brooks AFB, TX, Report USAFSAM-TR-85-73, 1986 [IEEE-1715]
- [14] A. Hirata et. al. *IEEE Trans. on Microwave Theory and Technique*, Vol. 51, pp.1834-1841, 2003
- [15] A. Hirata et. al. *IEEE Trans. on Electromag. Comp.*, Vol.48, no.3, pp.569-578, 2006
- [16] IEEE Std C95.3-2002, IEEE recommended practice for measurements and computations of radio frequency electromagnetic fields with respect to human exposure to such fields, 100 kHz-300 GHz, Annex E, IEEE New York, NY (2002)
- [17] A. Bijamov, A. Razmadze, L. Shoshiashvili, K. Tavzarashvili, R. Zaridze, G. Bit-Babik, A. Faraone, "Advanced Electro-Thermal Analysis for the assessment of human exposure in the near-field of EM sources.", ICEAA'03 International Conference on Electromagnetics in Advanced Applications, September 8-12, 2003 Torino, Italy.,
- [18] R. S. Zaridze, N. Gritsenko, G. Kajaia, E. Nikolaeva, A. Razmadze, L. Shoshiashvili, A. Bijamov, G. Bit-Babik, A. Faraone, "Electro-Thermal Computational Suit for Investigation of RF Power Absorption and Associated Temperature Change in Human

Body", 2005 IEEE AP-S International Symposium and USNC/URSI National Radio Science Meeting, July 3-8, 2005, Washington DC, USA. p. 175

[19] M. J. Ackerman, "The visible human project", Proc. IEEE, vol. 86, pp. 504-511, March 1998

[20] P. A. Mason, J. M. Ziriak, W. D. Hurt, T. J. Walter, K. L. Ryan, D. A. Nelson, K. I. Smith, and J. A. D'Andrea. Recent advancements in dosimetry measurements and modeling Radio Frequency Radiation Dosimetry. B J Klauenberg and D Miklavcic Eds. (Dordrecht: Kluwer), pp 141–55 (2000)

[21] A. Taflove, Ed., Computational Electrodynamics: The Finite-Difference Time-Domain Method. Norwood, MA: Artech House, 1995

[22] S. Gabriel, R. W. Lau, and C. Gabriel, "The dielectric properties of biological tissues: III. Parametric models for the frequency spectrum of tissues," Phys. Med. Biol., vol. 41, pp. 2271-2293, 1996

[23] P. Bernardi, M. Cavagnaro, S. Pisa, and E. PiuZZi, "Specific Absorption Rate and Temperature Elevation in a Subject Exposed in the Far-Field of Radio-Frequency Sources Operating in the 10–900-MHz Range," IEEE Trans. Biomed. Eng., vol. 50, pp. 295–304, March, 2003

[24] V. Flyckt, B. Raaymakers and J. Legendijk, "Modelling the impact of blood flow on the temperature distribution in the human eye and the orbit: fixed heat transfer coefficients versus the Pennes bioheat model versus discrete blood vessels," Phys. Med. Biol. vol. 51, pp 5007-5021, 2006

[25] Q. Li, O. Gandhi, "Thermal Implications of the New Relaxed IEEE RF Safety Standard for Head Exposures to Cellular Telephones at 835 and 1900 MHz," IEEE Trans. Microw. Theory Tech, vol. 54, pp. 3146 - 3155, 2006

[26] A. Hirata, "Computational Verification of Anesthesia Effect on Temperature Variations in Rabbit Eyes Exposed to 2.45 GHz," Bioelectromagnetics, Vol. 27, pp. 602-612, 2006

[27] K. S. Cole and R. H. Cole: "Dispersion and absorption in dielectrics: I. Alternating current characteristics.", Journal of Chemical Physics, April 1941, pp.341-351

[28] K. Caputa, M. Okoniewski, and M. Stuchly, "An algorithm for computation of the power deposition in human tissue", IEEE Antennas Propagat. Mag., vol. 41, pp. 102-107, June 1999

[29] H. H. Pennes, "Analysis of Tissue and Arterial Blood Temperature in the Resting Human Forearm," J. of Applied Physiology, Vol. 1, pp. 93-102, 1948

[30] P. Bernardi, M. Cavagnaro, S. Pisa, and E. PiuZZi, "Specific absorption rate and temperature increases in the head of a cellular-phone user," IEEE Trans. Microwave Theory Tech., vol 48, pp. 1118-1126, July 2000

[31] A. Taflove and M.E.Brodwin, "Computation of the electromagnetic fields and induced temperatures within a model of the microwave-irradiated human eye", IEEE Trans. Microwave Theory Tech, vol. MTT-23, pp. 888-896, Nov. 1975

[32] P. Bernardi, M. Cavagnaro, S. Pisa, and E. Piuzzi, "SAR Distribution and Temperature Increase in an Anatomical Model of the Human Eye Exposed to the Field Radiated by the User Antenna in a Wireless LAN", IEEE Trans. Microwave Theory Tech., vol. 46, December 1998